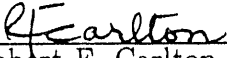


NUCLEAR STRUCTURE STUDIES *via* NEUTRON INTERACTIONS

Progress Report
1 July 1991 - 30 June 1992


Robert F. Carlton
Principal Investigator
Dept. of Chemistry & Physics


Ramona Rice, Director
Budget & Systems Planning


DISCLAIMER

This report was prepared as an account of work sponsored by an agency of the United States Government. Neither the United States Government nor any agency thereof, nor any of their employees, makes any warranty, express or implied, or assumes any legal liability or responsibility for the accuracy, completeness, or usefulness of any information, apparatus, product, or process disclosed, or represents that its use would not infringe privately owned rights. Reference herein to any specific commercial product, process, or service by trade name, trademark, manufacturer, or otherwise does not necessarily constitute or imply its endorsement, recommendation, or favoring by the United States Government or any agency thereof. The views and opinions of authors expressed herein do not necessarily state or reflect those of the United States Government or any agency thereof.

Middle Tennessee State University
Murfreesboro, Tennessee 37132
January 1992

Prepared for
THE U.S. DEPARTMENT OF ENERGY
Under Contract No. DE-FG05-86ER40293

MASTER


DISTRIBUTION OF THIS DOCUMENT IS UNLIMITED

NOTICE

This report was prepared as an account of work sponsored by the United States Government. Neither the United States nor the United States Department of Energy, nor any of their employees, nor any of their contractors, subcontractors, or their employees, makes any warranty, express or implied, or assume any legal liability or responsibility for the accuracy, completeness, or usefulness of any information, apparatus, produce or process disclosed or represents that its use would not infringe privately owned rights

ABSTRACT

Research performed consisted of: (1) publication of a theoretical paper for the $n+^{40}\text{Ar}$ system; (2) submission of a paper on the R-matrix analysis of the neutron total cross section data for the $n + ^{208}\text{Pb}$ system, up to an energy of 1.7 MeV; (3) extension of the analysis of neutron scattering and total cross section data for $n + ^{54}\text{Fe}$ up to an energy of 1 MeV, with J^π values confirmed in most cases by differential scattering data; (5) porting of most of the analysis programs used in the research program to the RISC/6000 workstation.

I. Introduction

Efforts during the reporting period have concentrated mainly on refinement of the analysis of total cross section data for three different target nuclei (^{208}Pb , ^{48}Ca and ^{54}Fe), aimed at the elimination of ambiguities in J^π assignments from the preliminary analyses and the development of a more nearly consistent set of model parameters. Three papers are in varying stages of completion for these nuclides and it is anticipated that one of these, likely on ^{208}Pb , will have been submitted by the end of the reporting period. Systematic efforts have continued on the part of statistical analysis programs, used as tools in the research program, to the environment of the RISC workstation.

Analysis of the total and differential scattering cross section data for the nucleus ^{54}Fe has been extended to the limit of 1 MeV, imposed by resolution. This has been a tedious process wherein, for each resonance in the total cross section, the measured and predicted scattering cross sections have been compared, with the latter assuming all J^π values through $5/2^+$. In many cases this was repeated for a different J^π value of an adjacent resonance when the cross section was likely to be characterized by resonance-resonance interference. Results for the 0-1 MeV region are presented in this report.

A technique has been developed for use in the determination of R-matrix external R-functions which ensures, that for each partial wave, the deduced parameters will properly account for the resonance-potential scattering interference for all resonances of that J^π over the entire energy range. This has also been found to be an aid to the determination of resonance J^π values. This approach has been applied to the ^{48}Ca data in order to clarify many of the preliminary assignments discussed in the last report and to extend the analyzed region to the the energy of the inelastic threshold. Final results are presented in this report. Similar efforts are in progress for the ^{208}Pb data and will be used as well in the ^{54}Fe study. This work will provide substantial information on these three nuclei to be used for comparison with the predictions of the dispersive optical model.

II. The $n - {}^{54}\text{Fe}$ System

Collaborator: J. A. Harvey

Results were given in the previous report for resonance analysis up to a neutron energy of 0.5 MeV. Detailed analysis of neutron total cross sections, combined with corroborative scattering cross sections is nearing completion up to 1 MeV. At higher energies the resonances are too close together to permit reliable analysis and J^π assignments. A total of approximately 350 resonances have been identified in this region and spin assignments have been made for most. The spectrum above 500 keV is dominated by s-wave resonances as shown in Figs. 1-2. This is similar to what we found below 500 keV, as reported in the previous report¹. An interesting feature of the $s_{1/2}$ -partial wave is the change of the hard-sphere phase shift with increasing energy as evinced by the resonances occurring as peaks in the region below 500 keV and as dips in the region above this energy. The smooth curve represents the R-matrix parametrization of the data. The dashed curve shows the s-wave contribution. Superposed on this major structure are numerous p- and d-wave resonances. Thus the s-wave interaction has by far the greater strength while the level density is greater for the other partial waves. From the combined analysis we have obtained resonance parameters and external R-functions, for each partial wave up to $d_{5/2}$.

The spin and parity identifications in the present work have been made possible by elastic scattering data measured at the 200-m flight path of the ORELA facility. Measurements at angles of 39° , 55° , 90° , and 160° have been compared to a Legendre expansion of the cross section,

$$\sigma(E, \theta) = \sum_L B_L P_L(\theta),$$

with the coefficients, B_L , determined from the phase shifts obtained from the R-matrix formalism. The J^π assignments have been based upon the requirement that the phase shifts corresponding to a given assumed spin reproduce the resonance asymmetry, and that the scattering cross sections at four different angles agree with predicted values. The conclusive nature of the of J^π assignments is seen in Fig. 3 where the scattering results are shown for a resonance whose neutron width was below the level necessary to manifest resonance asymmetry in the total cross section and thus determine the spin on

that basis alone. The data and calculations for the different angles in the lower portion, and for different J^π values in the upper portion have been offset for comparison purposes. Any of the attempted spins are acceptable from consideration of the total cross sections alone, but the scattering results clearly distinguish this resonance as $1/2^-$ in character.

Because of the size of the individual s-wave resonances there is strong correlation between the resonance parameters and the $R_{J\ell}^{\text{ext}}$ parameters. This required repeated adjustment of parameters in a given energy region following similar adjustment in other nearby regions until a consistent set of parameters was obtained for the entire region. The $R_{J\ell}^{\text{ext}}$ are parametrized as,

$$R_{J\ell}^{\text{ext}} = \bar{R}_{J\ell} - \bar{s}_{J\ell} \cdot \ln\left(\frac{E_u - E}{E - E_\ell}\right), \quad (1.1)$$

where

$$\bar{R}_{J\ell} = \alpha_{J\ell} + \beta_{J\ell} \cdot E. \quad (1.2)$$

The quantities, $E_u = 0$ and $E_\ell = 1$ MeV, are the upper and lower energy bounds for the investigation, respectively. The parameters α and β are adjustable in the R-matrix formalism and \bar{s} represents the average strength of resonances outside the analysis region and is taken to be equal to the observed strength.

The preliminary average resonance parameters obtained from the analysis of the 0 - 1 MeV region are summarized in Table I. Since the analysis is not complete we have not separated the different J-values for $p-$ and $d-$ wave resonances.

Table I. Preliminary Average Parameters for $n + {}^{54}\text{Fe}$ up to an energy of 1 MeV.

J^π	N^{obs}	$\langle g\Gamma_n^0 \rangle$ (keV)	$\langle D \rangle$ (keV)	S^ℓ ($\times 10^4$)
$1/2^+$	52	0.011 (3) ^a	17.8 (13)	6.2 (13)
$\ell = 1$	104	0.0084 (4)	7.7 (4)	0.38 (6)
$\ell = 2$	127	0.011 (4)	6.7 (3)	3.1 (4)

^aIn our notation $0.011 (3) \equiv 0.011 \pm 0.003$, etc. Corrections have not been made for estimates of missing resonances.

Fig. 4 shows the cumulative reduced neutron width vs. neutron energy for $s-, p-,$

and d -waves, with the s -wave results showing a decrease in strength with energies above 500 keV. This is not due to our missing s -wave resonances, but more likely a consequence of passing over the peak in the $3s$ size resonance as the neutron energy increases. The Porter-Thomas test confirms that few resonances are missed in the analysis. These preliminary results have not been corrected for missing resonances, but resonances missed or missassigned will be small and the strength functions will not be significantly affected. In most cases of small resonances where the total cross section results were completely insensitive to J^π , the scattering cross sections were unambiguous in the spin and parity required. In the case of larger resonances, the resonance asymmetry in the total cross section established the J^π value with the result that more than 80% of all resonances were given firm J^π assignments. This work, when completed, will provide average resonance parameters for individual partial waves from $1/2^+ - 5/2^+$. The large number of resonances observed and the identification of the spins and parities of the levels involved will permit an interpretation of the level densities and a determination of parameters of the back-shifted Fermi gas model. This will be the subject of the interpretation of the results.

III. The $n - {}^{48}\text{Ca}$ System

Collaborator: C. H. Johnson

Examination of the external R -functions during the interpretation of the results reported previously² revealed inconsistencies in systematic trends which were associated with incorrect assignment of spin or parity to some of the resonances. This resulted in a re-evaluation of the J^π assignments and the R -functions up to the 3.5 MeV limit of the previous report and an extension of the analysis to 3.9 MeV, the inelastic threshold for the reaction.

The resulting ${}^{48}\text{Ca}$ cross section is shown in Figures 5 and 6. The data uncertainties are less than the size of the circles, which represent the cross section and the curve through the data corresponds to a R -matrix parametrization of the data. Spin and parity assignments have been made primarily on the basis of interference asymmetries. For resonances too small to show interference with the R^{ext} , resonance-resonance interference was used to establish spins when near a large resonance of like

spin and parity. An example of this process of J^π assignment is shown in Fig. 7. The curve beneath the data corresponds to the $d_{5/2}$ partial wave contributions to the total cross section and illustrates the interference between both the resonances and the potential scattering cross section. The small resonance at 1230 keV only manifests asymmetry because of its close proximity to the adjacent resonance at 1550 keV. The large $d_{5/2}$ strength in this nuclide has thus permitted us to establish a nearly complete set of resonances for this J^π . The completeness of the sets of other partial waves may be less unambiguous. From the complexity of the cross section in the 2-4 MeV region one can surmise that not all resonances could be assigned definitive J^π values, but for the s-, p-, and d-waves most assignments are defensible on the basis of either peak cross section values, resonance-potential scattering interference, or reproducing cross section minima between resonances.

III. A. Data Analysis

We previously³ used a large boundary radius (7.5 fm) for the resonance analysis in order to be outside the polarizing forces when comparing the observed reduced widths with the single-particle values. Since the present work is devoted to a study of the scattering phase shifts, we adopt the conventional channel radius, namely, $a = 1.45A^{1/3} = 5.27$ fm. This will permit comparison of model predictions of the very similar work on $^{40}\text{Ar} + n$. This certainly provides for more definitive fitting of the data since we avoid the serious interference of the levels with the large R-function associated with the large channel radius. The larger radius resulted in a lowering of the $d_{5/2}$ - and s-wave single particle strength functions into the region of analysis, thus complicating the energy dependencies of the external R-functions and strength functions. A smaller boundary radius pushes the d- and s-wave strength function peaks to a higher energy such that these functions are well behaved in our region.

We previously used the R-matrix boundary condition, $B - S(E) = 0$, except for $d_{5/2}$ for which we used the condition, $B = \text{constant}$. This was because the energy shift, $S(E)$, could change considerably in the width of the very large $d_{5/2}$ resonances. In this work we have adopted, for all partial waves, the boundary condition,

$$B_{J^\pi} = S_{J^\pi}(1560 \text{ keV}).$$

III. B. Average Properties.

The average properties of interest in the present analysis include the level spacings, the strength functions and the R^{ext} functions. Their interest lies in the connection between these properties and the optical model potential.

(i.) LevelSpacings

To correct for the missing levels we assume that the observed reduced widths are drawn from Porter-Thomas (PT) distributions. Results are presented in Figs. 8 & 9. The new analysis resulted in the identification of several additional s-wave and p-wave resonances. Histograms are shown for all the partial waves and the solid curves are the expected distribution assuming no missed resonances. The dashed curves are from the PT distributions which best fit the data. From the extrapolation of the dashed curves to $x=0$ we find $N^m = 0, 2, 7, 8, 2$ missed resonances for the $1/2^+, 1/2^-, 3/2^-, 3/2^+, 5/2^+$ data sets, respectively. Based on these numbers and the observed number of levels, $N_{\ell J}^{obs}$, we present in Table II the level spacings obtained from the level densities, calculated from the expression,

$$\rho_{\ell J} = (N_{\ell J}^{obs} + N_{\ell J}^m - 1)/(E_{\ell f} - E_{\ell i}),$$

where $E_{\ell f}$ and $E_{\ell i}$ are the highest and lowest energy resonances in the (ℓ, J) data set. The J^π values for the narrow resonances at 1391, 1613, 1922, 2356, and 2483 keV could not be conclusively established. Attempts to include them in the various spin groups on the basis of the Dyson-Mehta Δ_3 statistic were unsuccessful. These observed resonances and others not included, but possibly supported by the total cross section data, suggest that our data set is nearly complete as estimated by the PT distributions.

The histogram in Fig. 10 represents the cumulative number of levels *versus* energy for the $d_{5/2^-}$ and $d_{3/2^-}$ partial waves. It is seen that the slope of the histogram for the $d_{5/2^-}$ partial wave is increasing with increasing energy as would be expected. Models for describing nuclear level densities usually concentrate on the backshifted Fermi-gas model. Since the $d_{5/2^-}$ sample is, statistically speaking, the best, we have applied the model to this data set. In the model the excitation energy U is measured from a fictive ground-state energy U_0 ,

$$U = E + (S_n - U_o),$$

where S_n is the neutron separation energy, which in the case of $n + {}^{48}\text{Ca}$ is 5.146 MeV. The total density summed over J is

$$\rho_{tot}(U) = \frac{1}{12\sqrt{2}\sigma} \frac{\exp[-2(a_o U)^{1/2}]}{a_o^{1/4} U^{5/4}}.$$

and the density for a given J is

$$\rho_J(U) = \rho_{tot}(U) \frac{(2J+1)\exp[-\frac{(J+\frac{1}{2})^2}{2\sigma^2}]}{2\sigma^2}.$$

The spin cut-off factor σ^2 has an energy dependence given by

$$\sigma^2 = 0.088\sqrt{(aU)} A^{1/3},$$

where A is the atomic mass number. The two parameters a_o and U_o are then adjusted to fit the number of levels in the unbound region where the resonance analysis has been accomplished and in a selected region of the bound energy levels. For the latter we use the number of low-lying states reported in the Nuclear Data Tables 48, 581 (1986) in the energy range 3.3 - 4.3 MeV. For the unbound region we could use the number of observed resonances, corrected for missed levels as discussed above, for any of the partial waves. We have chosen the $d_{5/2}$ levels because the uncertainty due to missed levels is thereby minimized. The parameters of the model are then obtained from a least squares adjustment subject to the following constraints on the excited levels in ${}^{49}\text{Ca}$,

$$N^{ex} = \int_{3.3}^{4.3} dU \rho_{tot}(U) = 2$$

and the number of resonances observed,

$$N(5/2^+) = 1/2 \int_0^{3.9} dU \cdot \rho_{5/2}(U) = 24.$$

The factor 1/2 is a result of the assumption that both parities for a given J are equally represented. We thus find $x_o = 4.10 \text{ MeV}^{-1}$ and $U_o = 0.25 \text{ MeV}$. These values, when used to calculate the level density for the other partial waves, give level densities consistent with the observed values, within uncertainty estimates of the PT test, and

thus provide some indication of the completeness of the other partial wave samples. To assess the uncertainty in the deduced parameters as a result of reliance upon only one J^π sample ($d_{5/2}$), parameters for each of the partial wave samples have been varied, in a similar manner, to fit that particular sample. The corresponding parameters differ from those obtained for the $d_{5/2}$ sample by no more than 10%.

(ii.) Strength functions

The strength functions $\tilde{s}_{\ell J}$ are related to the slopes of the cumulative reduced width versus energy distribution shown in Fig. 11 for s-, p-, and d-wave resonances. We have not corrected these strength functions for missing levels since our estimate of the effect of missing a few small resonances is negligible. We present the strength functions for each partial wave in Table II. As can be seen in Fig. 11 the s-wave strength expected on the basis of resonances below 2 MeV would be near zero as reported in our earlier study of this reaction. The onset of s-wave strength at this energy is consistent with single-particle predictions in that work. There it was predicted that any s-wave strength should be expected above 2 MeV. The s- and d- waves strengths are consistent with other nuclei in this mass region. For the p-waves, however, the results are low by a factor of two. The large $d_{5/2}$ strength is a consequence of the 2D state being just unbound. The lower value of those components which are further removed from the separation energy are related to the deeper binding in the case of the $p_{3/2}$ strength and the higher unbound position for the $d_{3/2}$ state.

TABLE II. Average level spacing and strength functions for $n + {}^{48}\text{Ca}$.

J^π	$N_{\ell J}^{obs}$	$N_{\ell J}^m$	$D_{\ell J}(\text{keV})^a$	$\tilde{s}_{\ell J}$
$1/2^+$	9	0	456 (84)	.12 (6)
$1/2^-$	6	2	464 (92)	.008 (5)
$3/2^-$	9	7	219 (30)	.007 (3)
$3/2^+$	14	8	129 (15)	.03 (1)
$5/2^+$	24	2	138 (15)	.48 (15)

^aIn our notation $456 (84) \equiv 456 \pm 84$, etc.

(iii.) External R-functions

For the case of a single open channel, the R-matrix reduces to a R-function. This function is a sum over all resonances with quantum numbers ℓJ , observed within the region of analysis, plus a smoothly increasing function of energy which describes the aggregate effect, within the region, of levels external to the region. It may be expressed as

$$R_{\ell J}(E) = \sum_{\lambda=1}^N \frac{\gamma_{\ell J \lambda}^2}{E_{\ell J \lambda} - E} + R_{\ell J}^{ext}(E),$$

where $\gamma_{\ell J \lambda}^2$ and $E_{\ell J \lambda}$ are free parameters representing the reduced neutron width and energy of the λ th resonance with angular momentum ℓ and J , and N is the corresponding number of resonances observed within the region.

The external R-function, $R_{\ell J}^{ext}$, represents the cumulative effect, within the fitted energy region, of resonances outside that region. If the resonances outside the region were known, their contribution would be included in the summation. This is not usually the case. The only requirement that can be placed on the $R_{\ell J}^{ext}$ is that they be increasing functions of energy. Thus any convenient function meeting that condition would be satisfactory. In addition we have some qualitative guidance from model calculations concerning the relative magnitudes for the various partial waves to which the experiment is sensitive. For energies well within the endpoints, a polynomial function of energy could be used. Resonances near the endpoints make significantly greater contributions and result in a departure from that simple form. In such cases a logarithmic function has been demonstrated to be adequate. This results in a more rapid increase in R^{ext} with energy near the endpoints and which is symmetric about the midpoint of the energy range. In the present case we do not expect the low-energy component of this symmetry to be present and have thus parametrized the $R_{\ell J}^{ext}$ by a linear (quadratic in the case of $p_{1/2}$) function of energy plus contributions from a series of fictitious "poles" located just above the upper energy. The free parameters of the R^{ext} are thus the coefficients of the linear portion, referred to as $\bar{R}_{J\ell}$, and the energies and reduced widths of the "poles".

We observed resonances above 3900 keV but because the inelastic channel opens at this energy and because the resolution was insufficient to separate adjacent resonances,

we have added to the linear portion a small number of terms of the same form as the addends above. The energies and widths of these "poles" were adjusted to provide the proper resonance asymmetries near the 3900 keV limit of analysis and held fixed during the remainder of the fitting process. General trends of the $R_{J\ell}^{ext}$ were thus established by adjusting the parameters of the $\bar{R}_{J\ell}$ to fit the asymmetry of two or more resonances of established J^π separated by large energy difference. For any model the $\bar{R}_{J\ell}$ generally increases with increasing energy except in the region of a strength function resonance. For the channel radius chosen, all $\bar{R}_{J\ell}$ except the $f_{5/2}$ increase rather slowly with energy. We obtain information on a given $\bar{R}_{J\ell}$: (1) at off-resonance energies where the cross section is zero for other contributing partial waves and (2) by fitting the detailed interference pattern of isolated resonances whose widths are greater than the resolution width at that energy.

Once the spins of low energy resonances were established, we deduced the low-energy $\bar{R}_{J\ell}$ values based on the fitting of the interference patterns for these resonances. The energy dependence of the $\bar{R}_{J\ell}$ values was established initially by fitting interference patterns in the 1300-1800 keV region, with the requirement that the off-resonance cross sections be properly and consistently described. This region contains resonances for each partial wave and in addition near 1200 keV the $d_{5/2}$ contribution to the off-resonance cross section is zero. While the cumulative effect of the contributing partial waves in this region is not unambiguous, the constraint that the interference patterns also be properly accounted for, ensures that the results are probably good. This fixed the $\bar{R}_{J\ell}$ (linear portion of the R^{ext}) parameters for each spin group.

The process of determination of these parameters served an additional purpose of confirming both the spin assignments for many of the resonances manifesting asymmetry and the internal consistency of the total parameter set. In addition an indication of the uncertainty of the parameters of the $R_{J\ell}^{ext}$ was obtained. In this process the energy region 0-4 MeV has been divided into as many as ten energy segments for fitting. Within a given segment the parameters of resonances internal to that segment were varied. In addition the parameters of the $\bar{R}_{J\ell}$ were varied for all partial waves manifesting measurable resonance-potential scattering interference within the region. This procedure served to corroborate the spin assignments for the resonances in the current segment. For example, when fitting a new energy segment with assumed J^π values and permitting the R-function parameters to vary, the failure of

the resulting least-squares parameters to be consistent with clearly established trends for that partial wave suggested an incorrect spin or parity assignment for a large resonance either within or just outside the segment energy. The second constraint imposed on the $R_{J\ell}^{ext}$ was that it must be an increasing function of energy. In this way we have obtained a self-consistent set of spin assignments which have much more validity than one based upon a fitting procedure which ignores the trend of off resonance potential scattering. While the resulting parameter set may not be unambiguous, as was discovered before we developed this procedure, it is definitely less uncertain than would be the case otherwise. From the plot of the R^{ext} shown in Fig. 12 the consistency of the final parameter set (indicated by the smooth lines) with the individual segment results allows us to establish overall uncertainties on the values. These are included in Table III with the parameters of the R^{ext} .

TABLE III. Parameters for the External R-functions, $R_{\ell J}^{ext \dagger}$ for $n + {}^{48}\text{Ca}$.

J^π	a	b (MeV^{-1})	c (MeV^{-2})	$E_{\ell J}$ (keV)	$\Gamma_{n\ell J}$ (keV)	$\Delta R^{\dagger\dagger}$
$1/2^+$	0.723	0.258		404	200	
$1/2^-$	-0.36	0.15	-0.012	402	10	0.008
$3/2^-$	-0.12	0.053		408	40	0.008
				391.4	14	
$3/2^+$	0.22	0.26				0.014
$5/2^+$	0.17	0.175		402	10	0.007
				406	20	
				410	10	
				413	25	
$5/2^-$	-0.15	-0.08				
$7/2^-$	0.24	0.15		391.5	2	

\dagger The parametrization is of the form

$$R_{\ell J}^{ext}(E) = a_{\ell J} + b_{\ell J} \cdot E + c_{\ell J} \cdot E^2 + \sum_{\lambda=1}^N \frac{\gamma_{\lambda\ell J}^2}{E_{\lambda\ell J} - E},$$

where N is the number of "poles" of a given ℓJ ; $\gamma_{\lambda\ell J}^2$ and $E_{\lambda\ell J}$ are their reduced widths and energies.

$\dagger\dagger$ The uncertainties were taken as the average fluctuations of segment results from entire-region results.

These preliminary results are to be devoted to a dispersive optical model analysis before the end of the current reporting period. This will involve, as in the case of $n + {}^{40}\text{Ar}$, the comparison of scattering functions and R-functions with model predictions for each individual partial wave. The model will use parameters deduced from extensive data on the $n + {}^{40}\text{Ca}$ system with suitable modification of the isovector potential for the different asymmetry coefficient.

IV. The $n - {}^{208}\text{Pb}$ System

Collaborator: R.R. Winters

Efforts on this nuclide have been focussed on firm J^π determinations for as many small resonances as possible. We have tested all resonances with uncertain assignments in two ways: (i) for each resonance all J^π values, over the entire range of values observed in the spectrum, *i.e.*, $1/2^+ - 5/2^+$, have been tested by minimizing the χ^2 through variation of the resonance and R^{ext} parameters; and (ii) checking for R^{ext} -consistency as parameters for each resonance are allowed to vary; as discussed above. While this approach is time consuming and has thus delayed the interpretation of this data, it is expected to result in improved integrity of the data set. This analysis, when completed, will be devoted to the dispersive optical model through comparison of scattering functions and R-functions with model predictions for each individual partial wave. The model will use parameters deduced from extensive data on the $n - {}^{208}\text{Pb}$ system. A paper is expected to be submitted near the end of the reporting period.

Figure Captions

- Fig.1 Total cross section for $n-^{54}\text{Fe}$ over the neutron energy range 400–700 keV. The solid line represents the R-matrix parametrization of the data.
- Fig.2 Total cross section for $n-^{54}\text{Fe}$ over the neutron energy range 700–1000. keV. The solid line represents the R-matrix parametrization of the data.
- Fig.3 Total and scattering cross sections for a small resonance in $n-^{54}\text{Fe}$. The circles in the scattering data correspond to an angle of 90° and the triangles to 160° . The solid line represents the prediction for $p_{1/2}$ interaction, and the short and long dashed lines correspond to $p_{3/2}$ and $d_{3/2}$ predictions, respectively. The successive cross section curves have been offset 1 MeV for plotting.
- Fig.4 Cumulative sum of reduced widths for s -, p -, and d -wave resonances observed in $n-^{54}\text{Fe}$.
- Fig.5 Total cross section for $n-^{48}\text{Ca}$ over the neutron energy range 100–2600 keV. The solid line represents the R-matrix parametrization of the data. The error bars on the data are less than the size of the circles.
- Fig.6 Total cross section for $n-^{48}\text{Ca}$ over the neutron energy range 2.6–4.0 MeV. The solid line through the data points represents the R-matrix parametrization of the data.
- Fig.7 A portion of the total cross section for $n-^{48}\text{Ca}$, showing resonance-resonance interference between the small $d_{5/2}$ resonance and the large nearby resonance of that same partial wave. The dashed line shows the $d_{5/2}$ contribution.
- Fig.8 Porter-Thomas test for missing s - and p -wave levels in $n+^{48}\text{Ca}$. The histograms give the observed distributions. The solid lines are the predicted results for zero assumed missing resonances and dashed curves give results for the estimated number of missing resonances.
- Fig.9 Similar to Fig. 8 for d -wave resonances.
- Fig.10 The cumulative number of observed resonances for d -wave resonances in $n+^{48}\text{Ca}$. The curves are calculated using the back-shifted Fermi-gas model for the nuclear level density. The parameters deduced from fitting the histogram for the $d_{5/2}$ levels were used to predict the results for $d_{3/2}$ levels.
- Fig.11 Cumulative reduced widths observed for s -, p -, and d -waves in $n+^{48}\text{Ca}$. The strength function is related to the slopes of lines drawn through these histograms.
- Fig.12 External R-functions for $n+^{48}\text{Ca}$. The line-connected squares represent values deduced from fitting over corresponding energy ranges and smooth curves correspond to fits to the energy-segment results. Smooth-curve parameters are given in Table III.

REFERENCES

- 1 R.F Carlton, DOE Progress Report, DE-FG05-86ER40293-5 (1991).
- 2 R.F. Carlton, DOE Progress Report, DE-FG05-86ER40293-6 (1990).
- 3 R.F. Carlton, J.A. Harvey, R.L. Macklin, C.H. Johnson, and B. Castel, Nuclear Physics A465, 274 (1987).

54 Fe

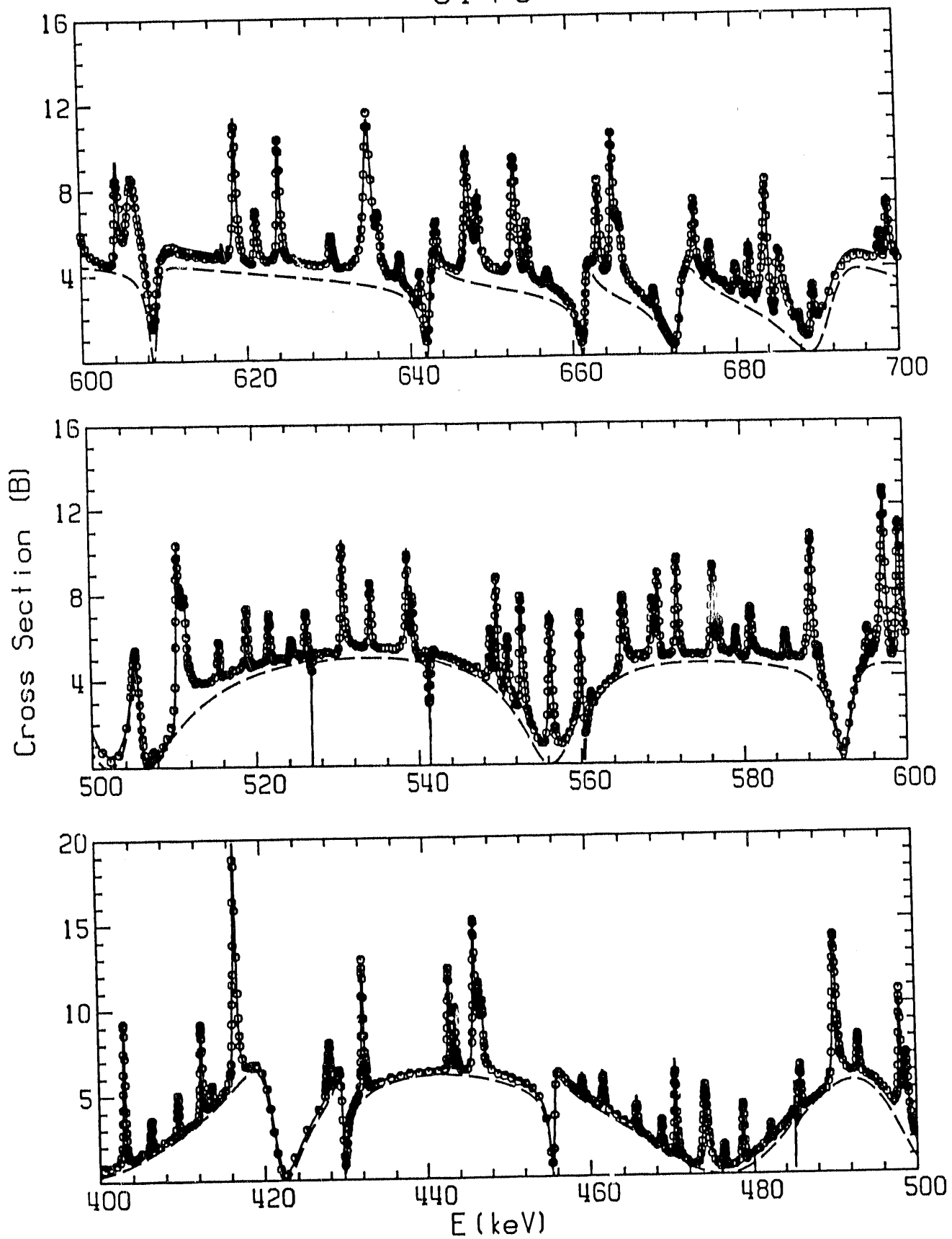


Figure 1

54 Fe

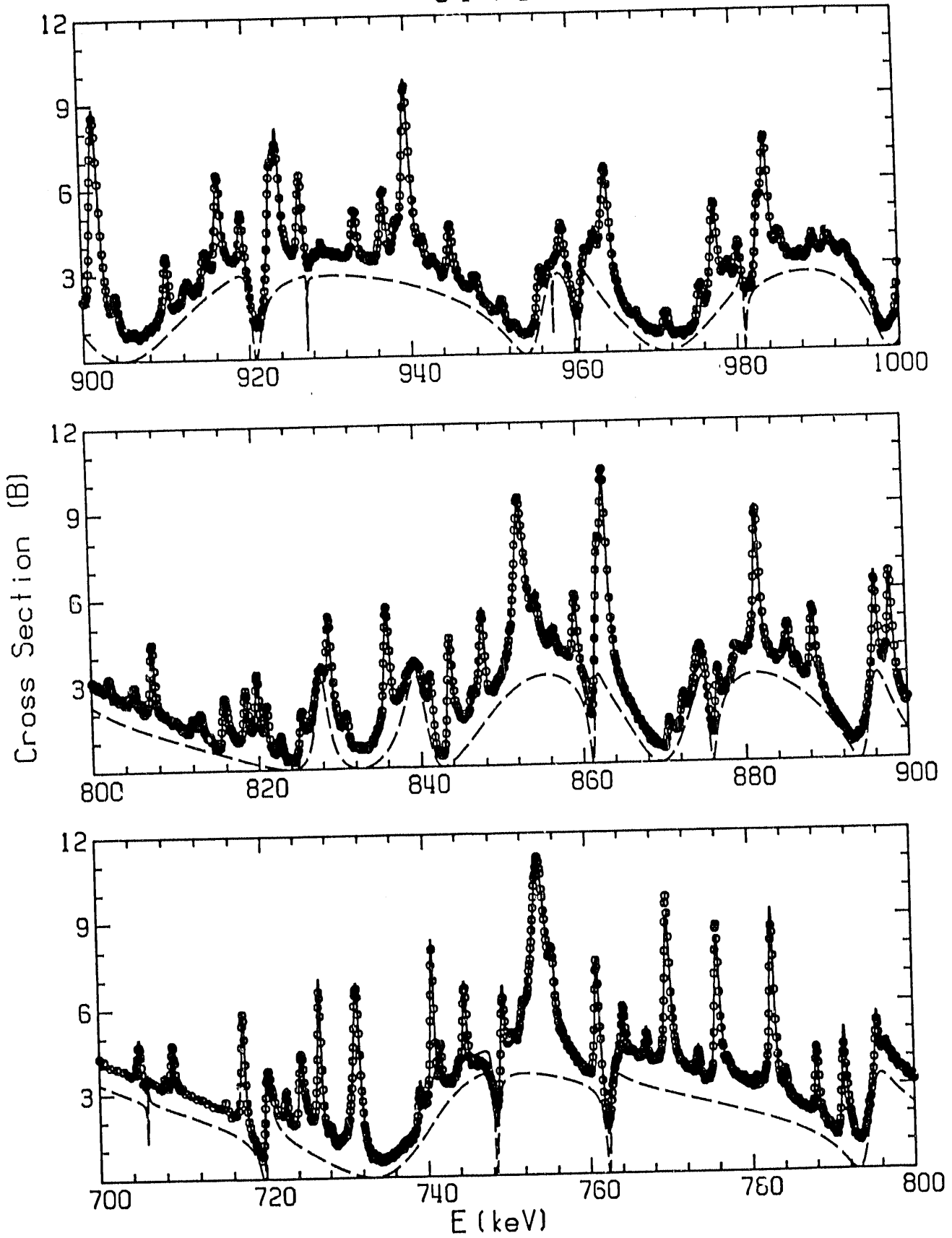


Figure 2

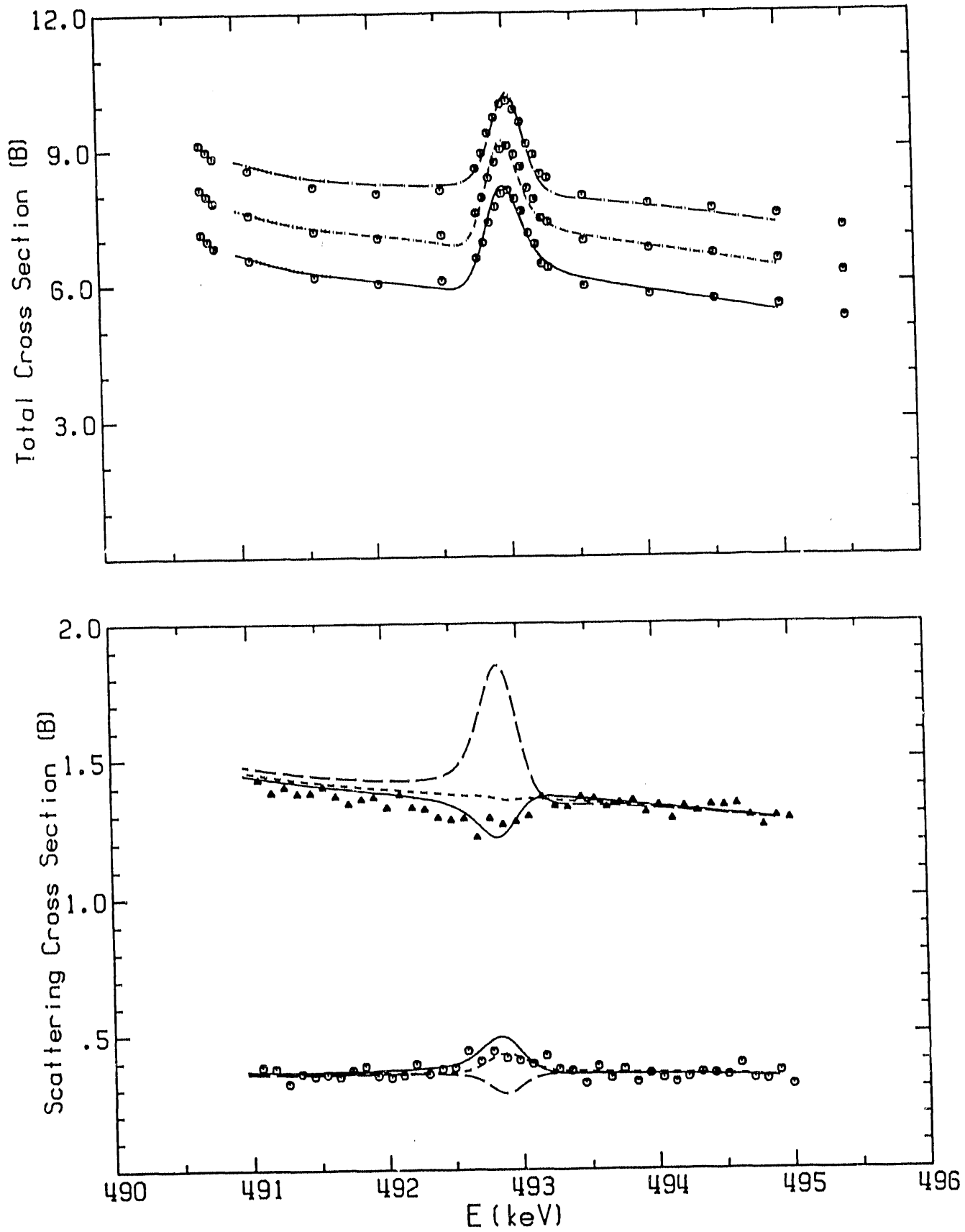


Figure 3

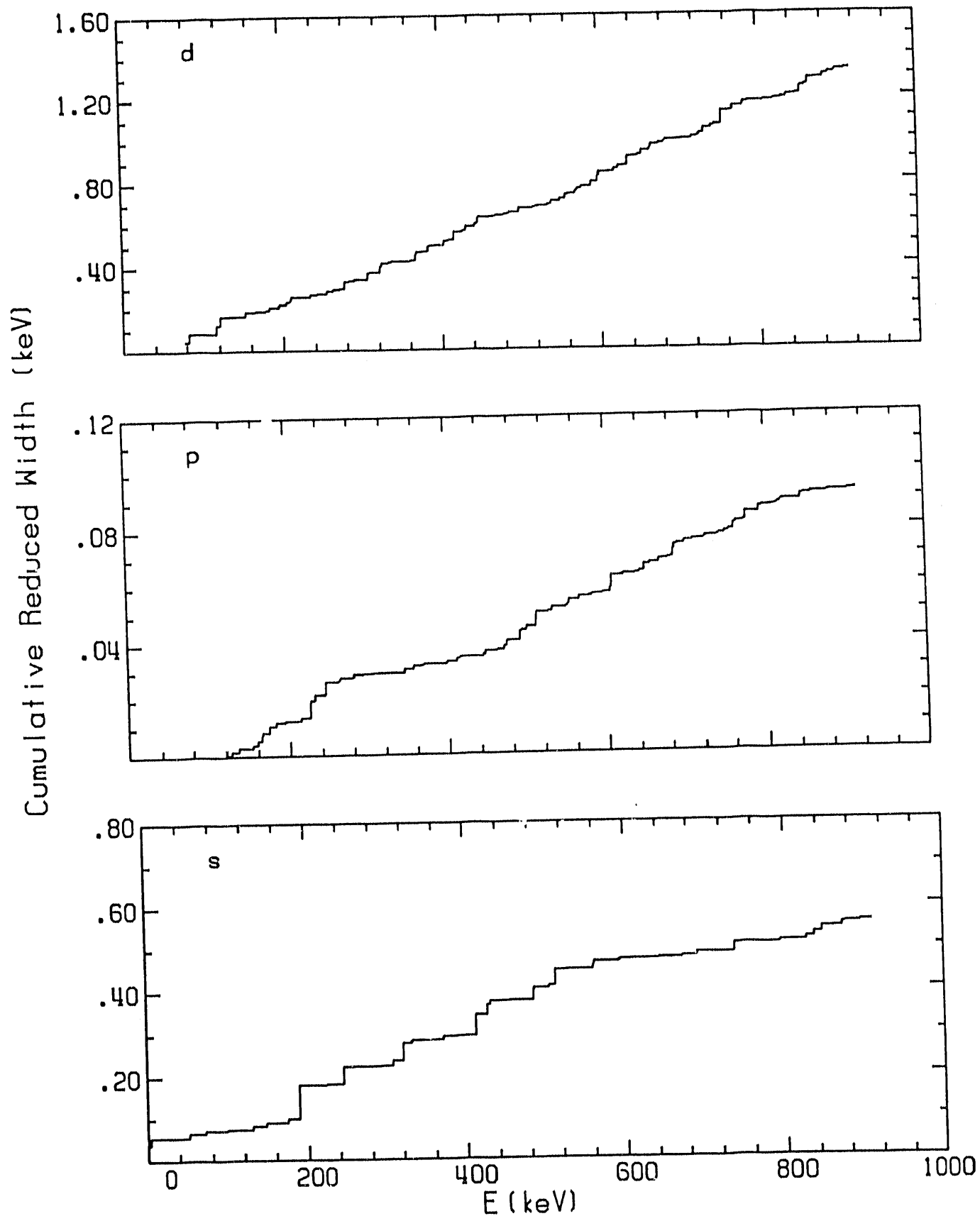


Figure 4

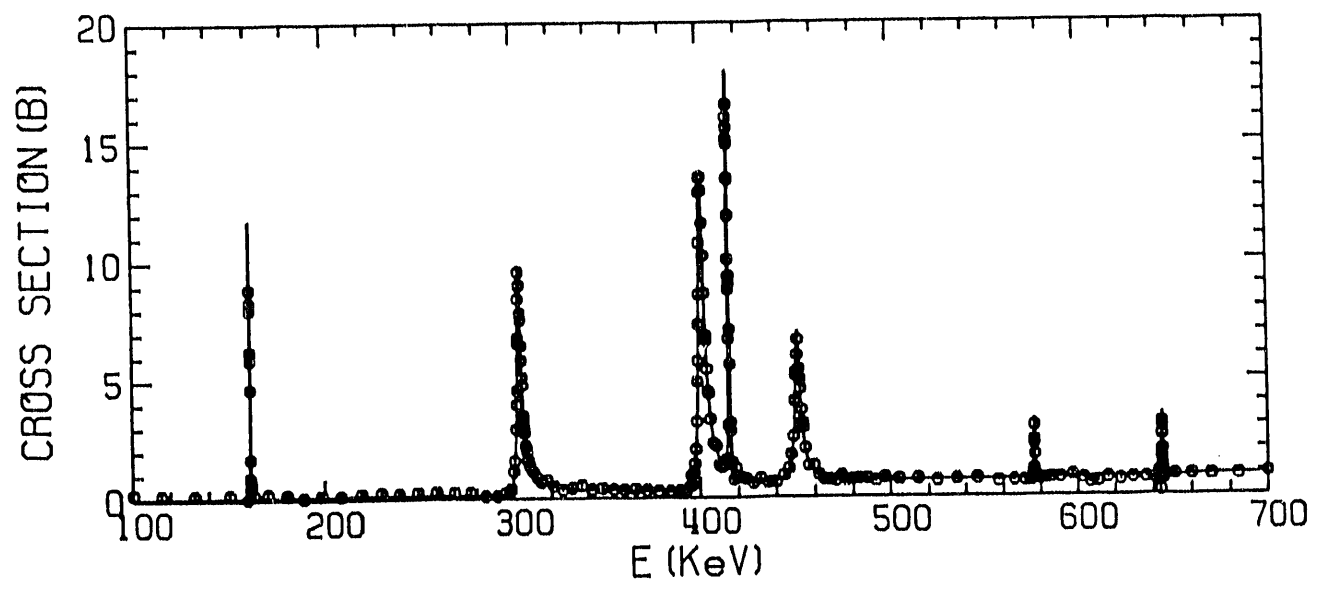
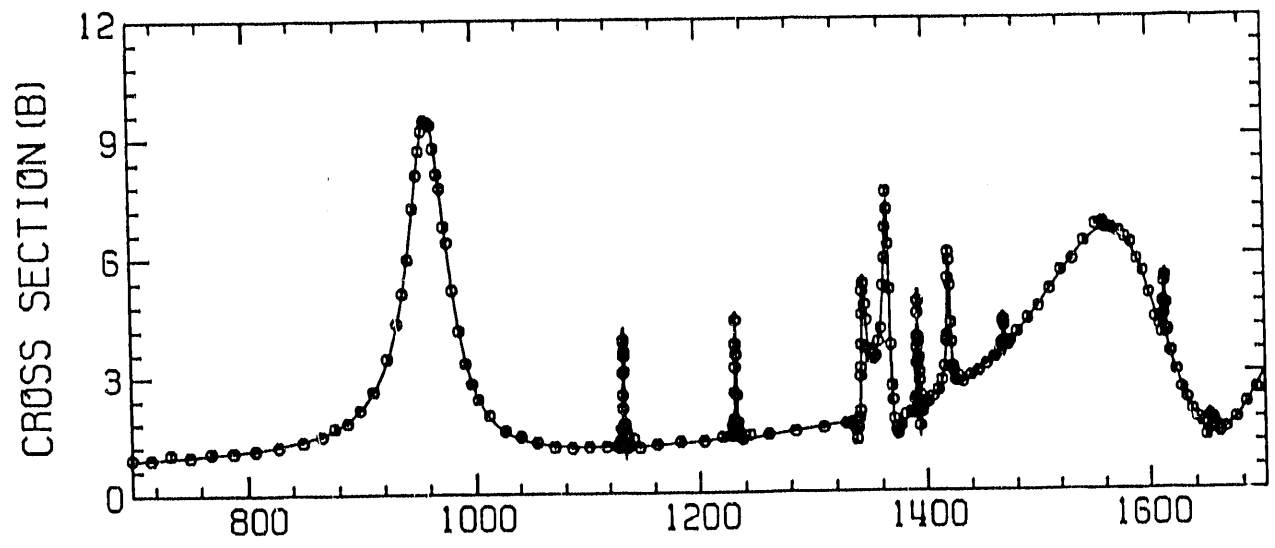
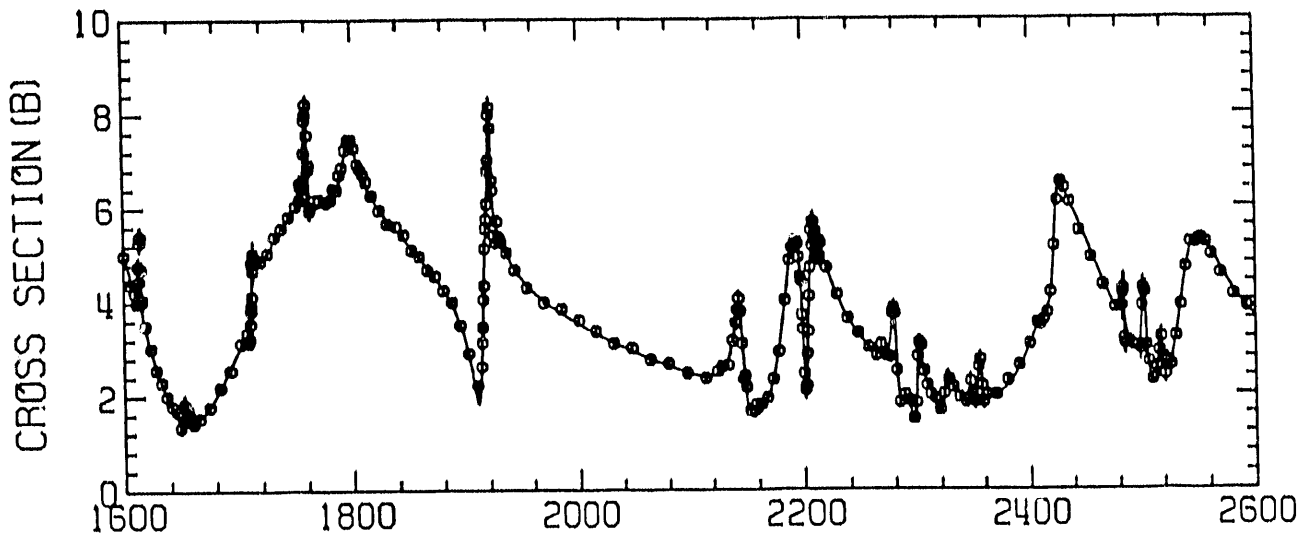


Figure 5

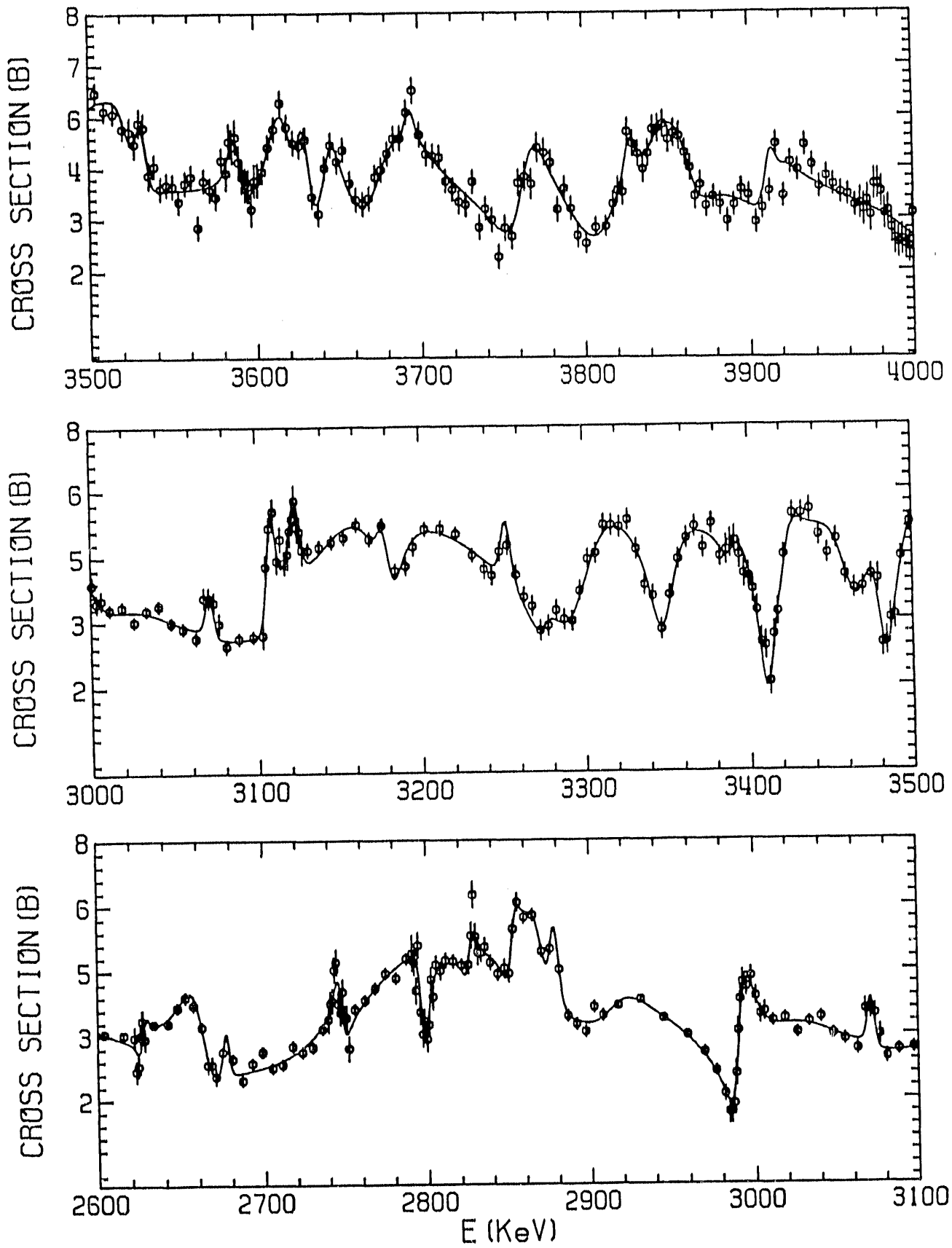


Figure 6

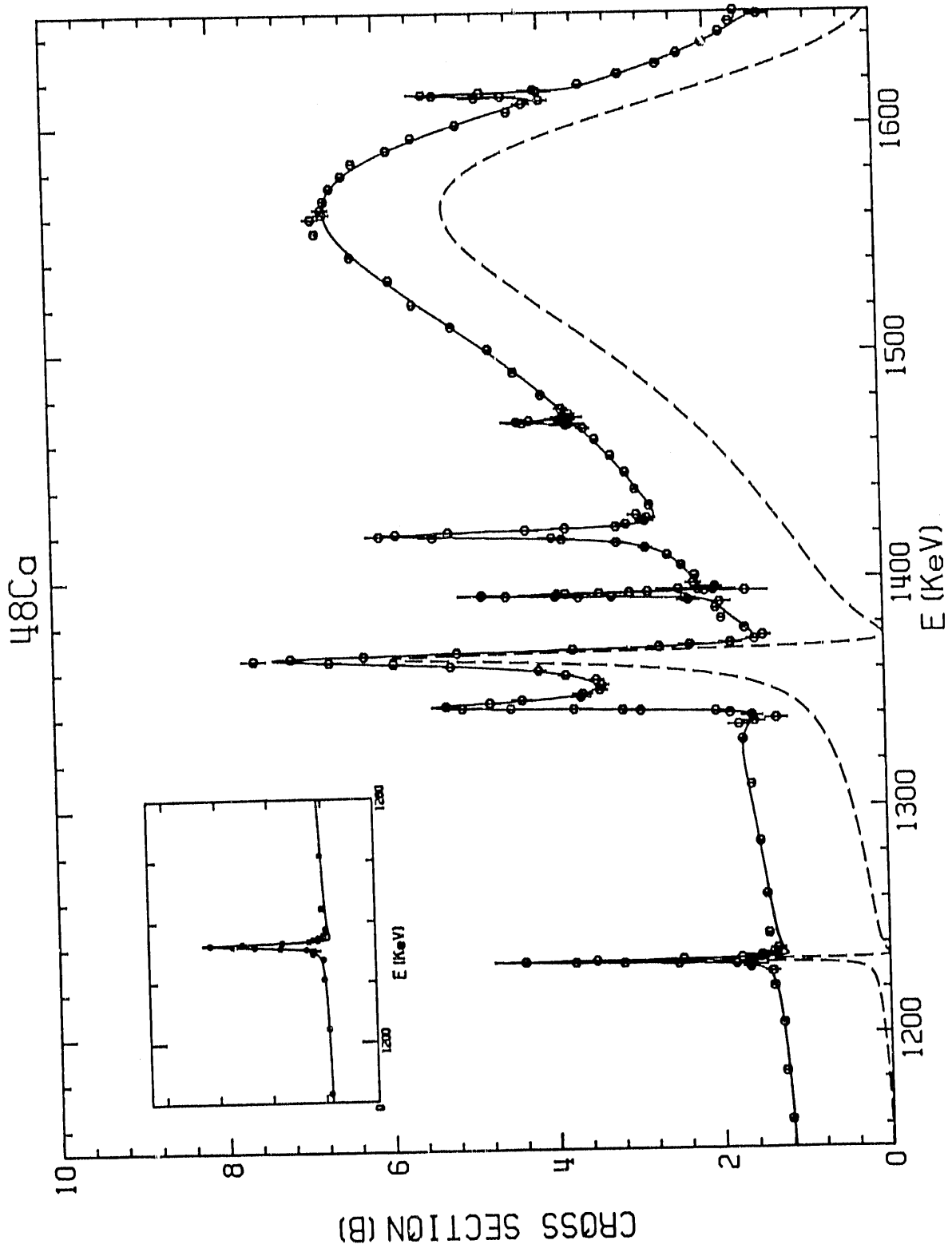


Figure 7

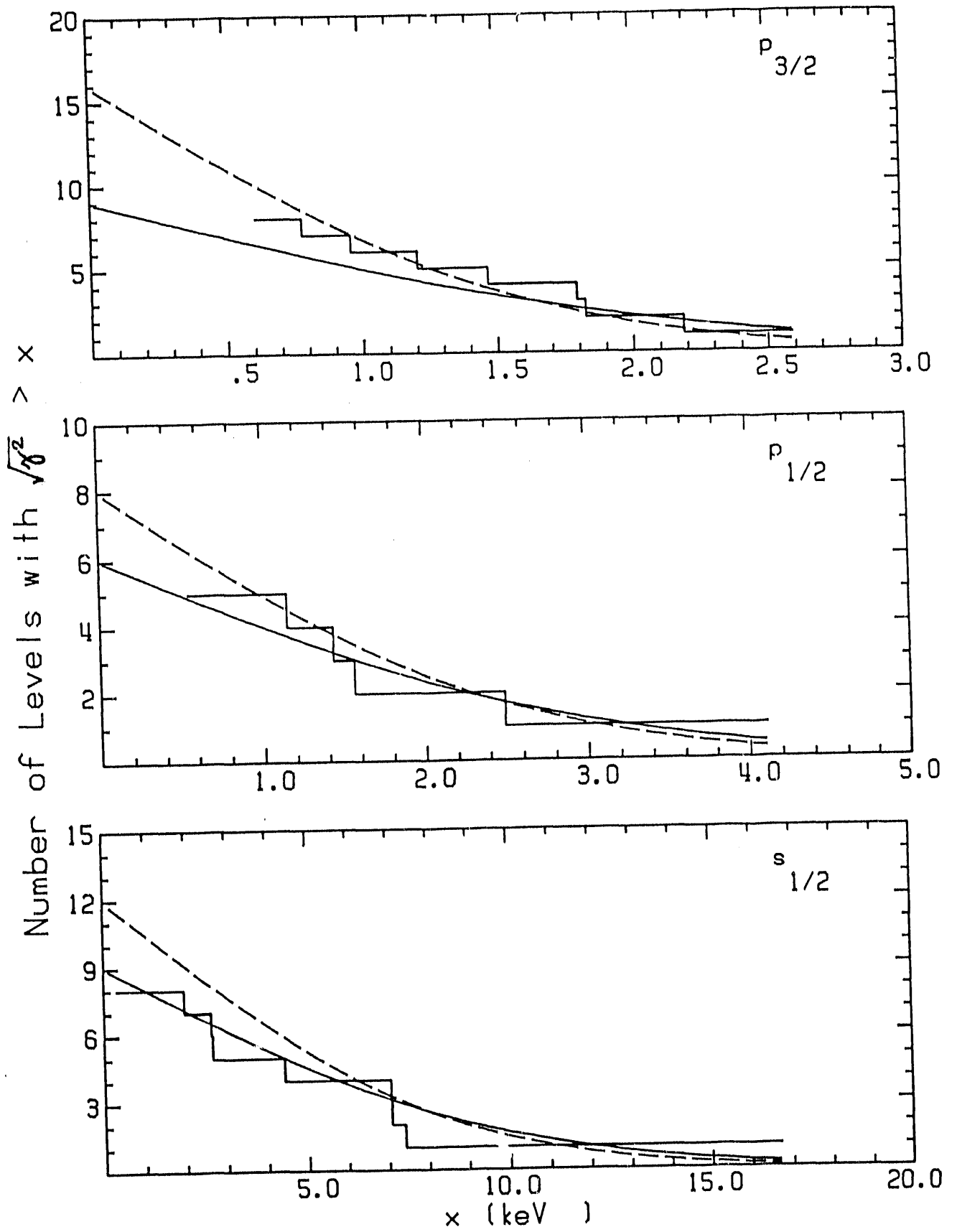


Figure 8

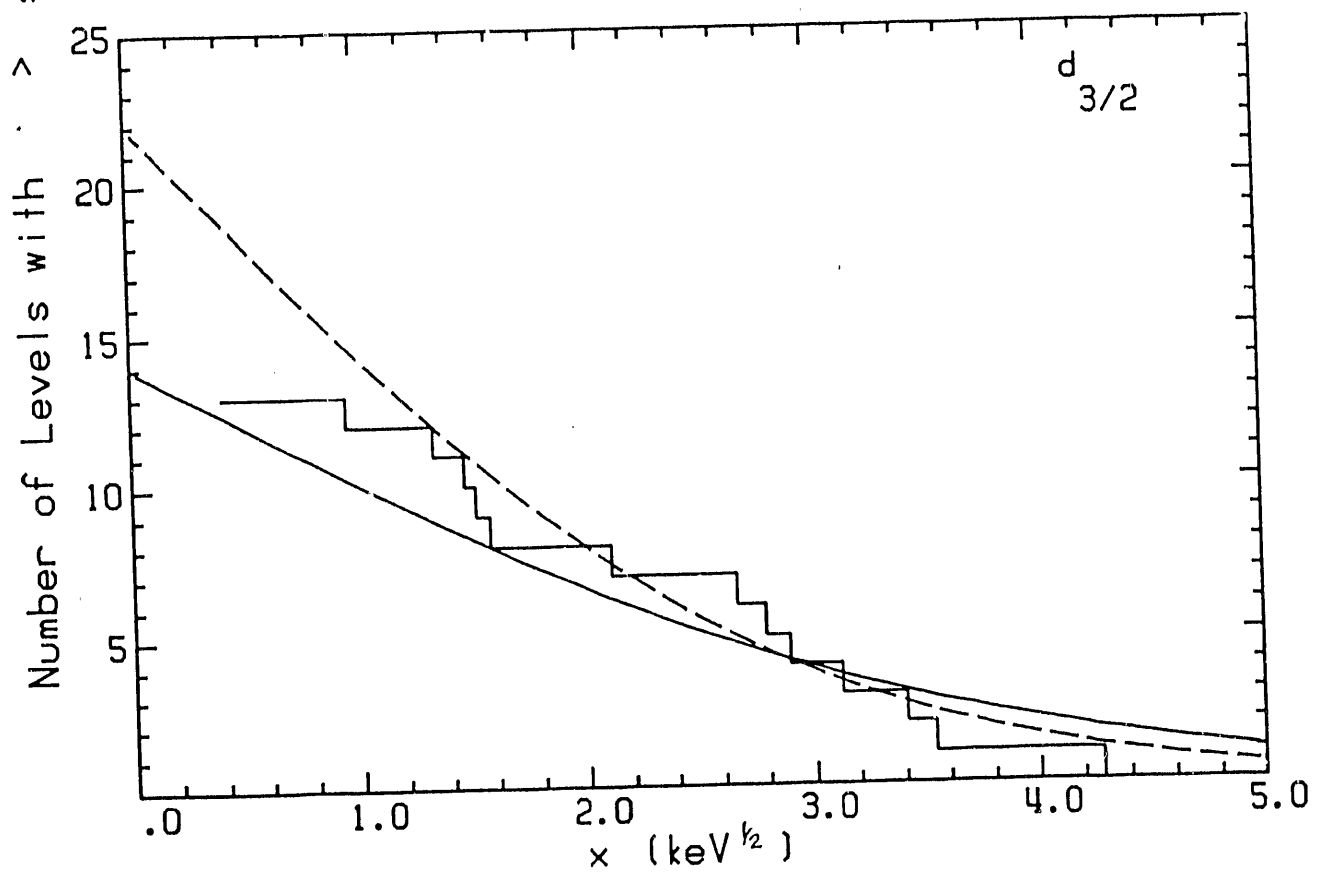
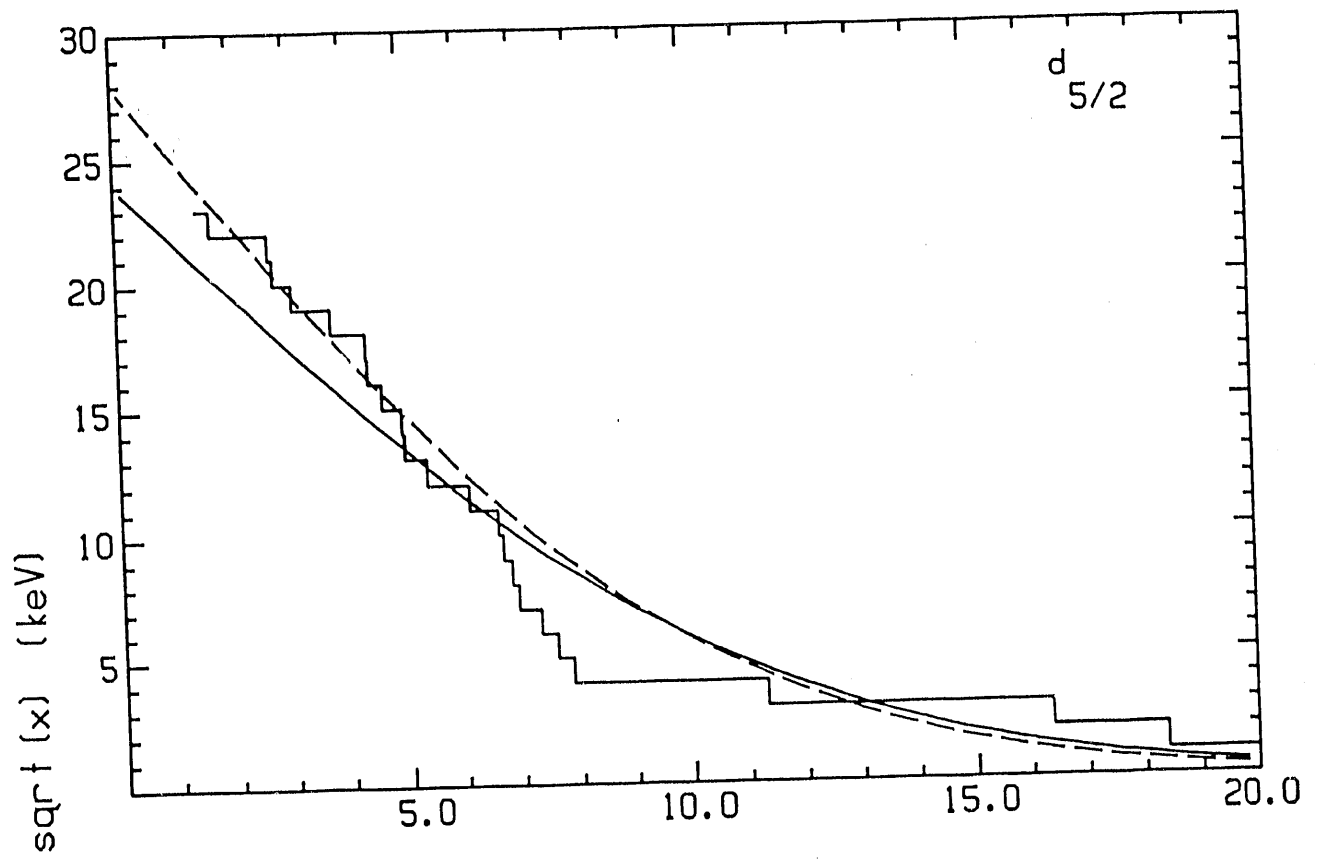


Figure 9

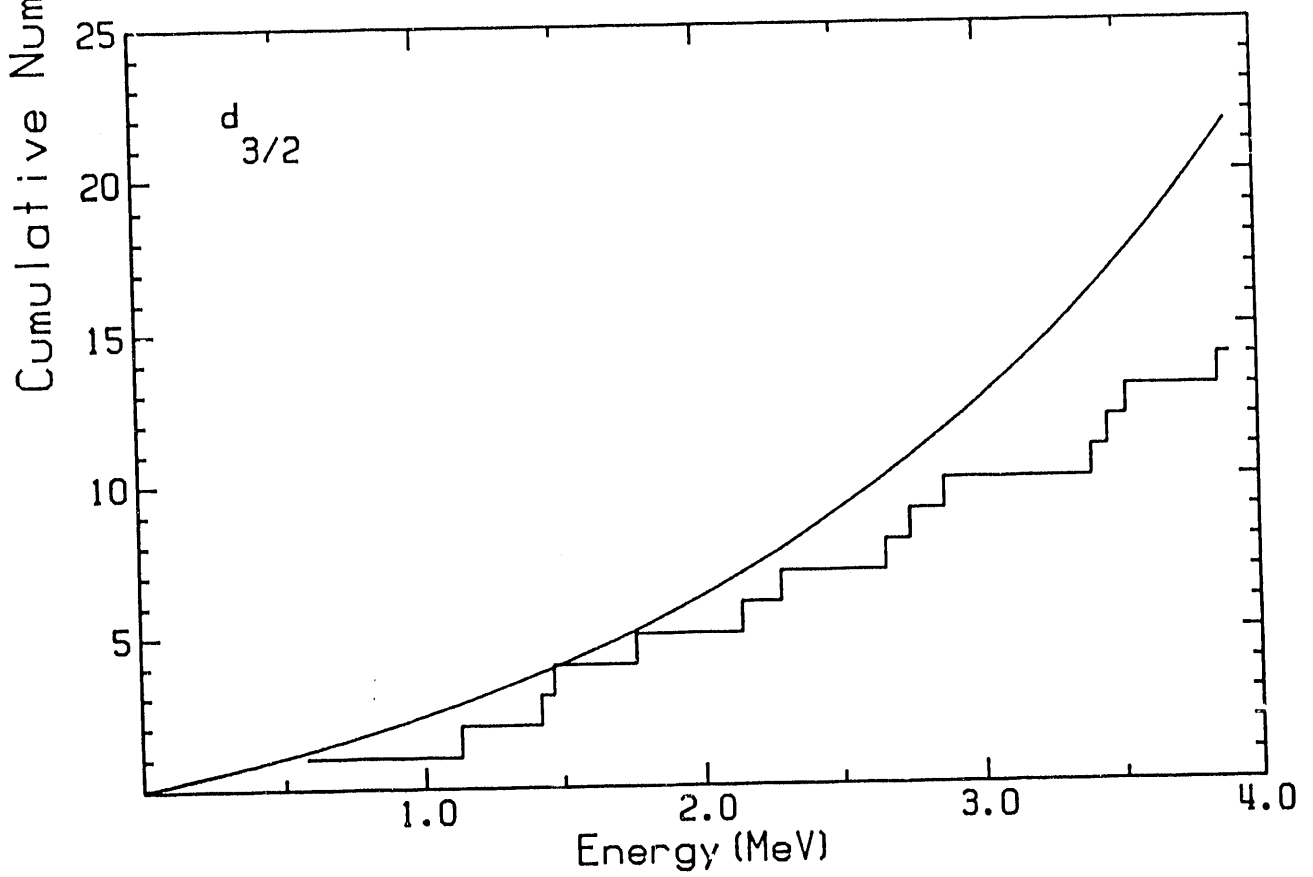
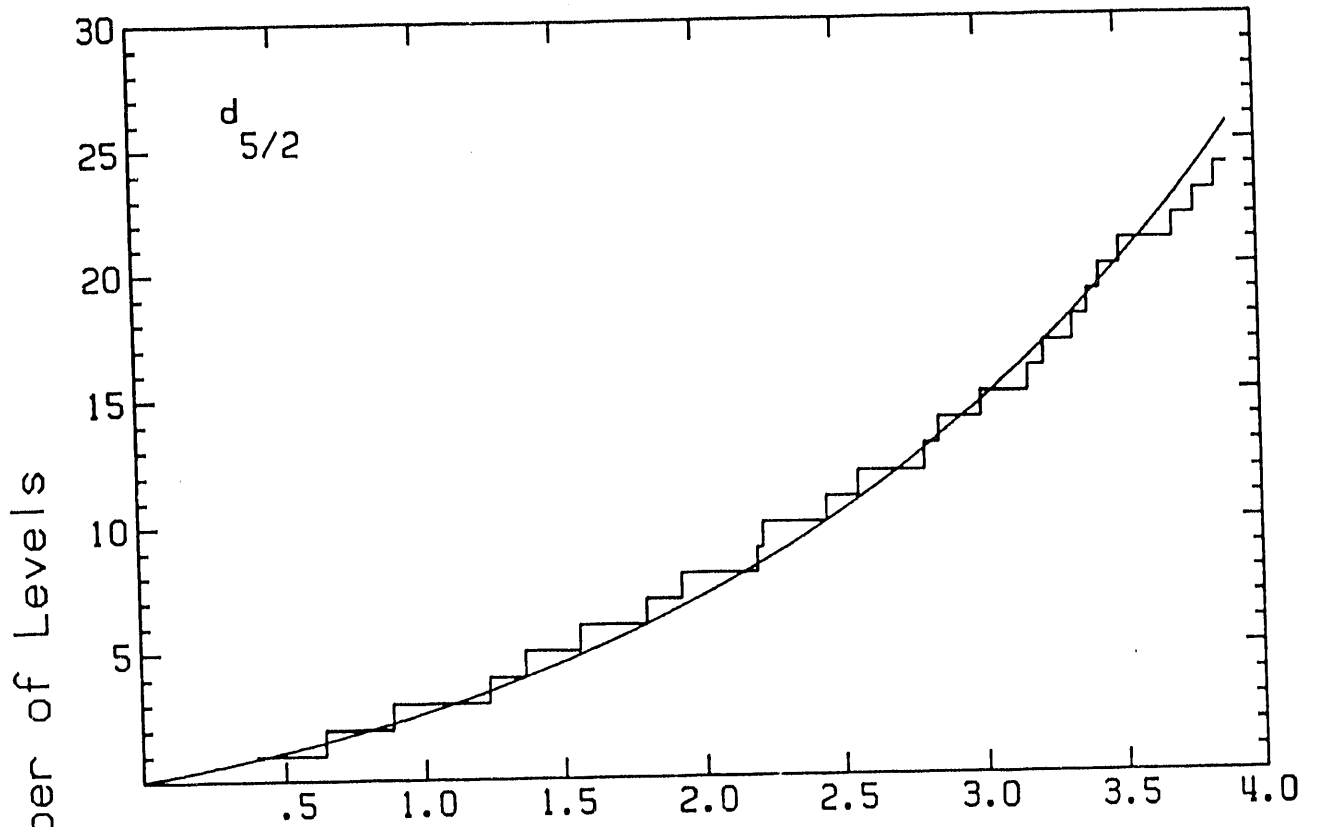


Figure 10

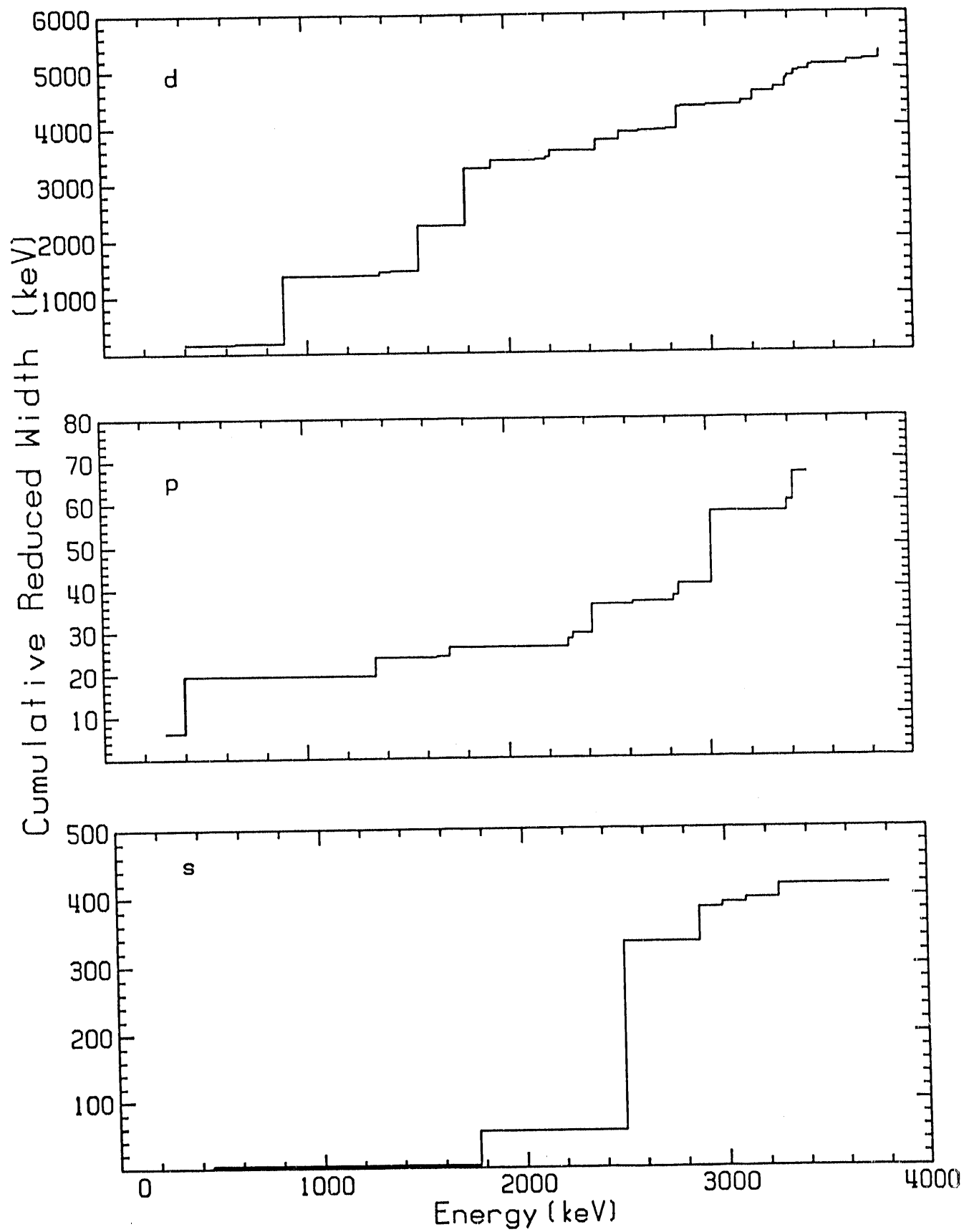
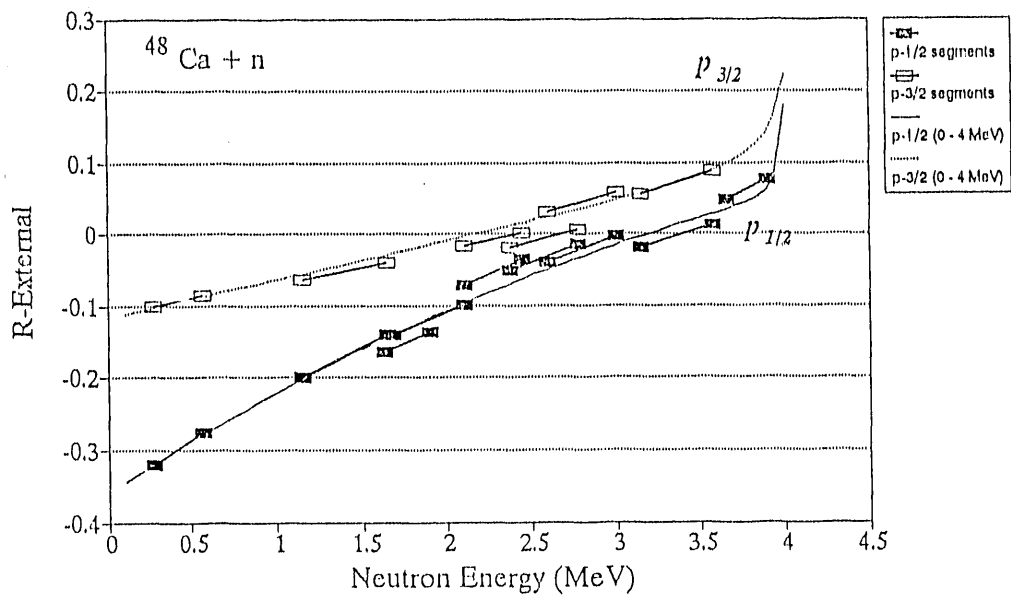


Figure 11

R-externals (including poles)
for segment- & entire region- fitting



R-externals (including poles)
for segment- & entire region- fitting

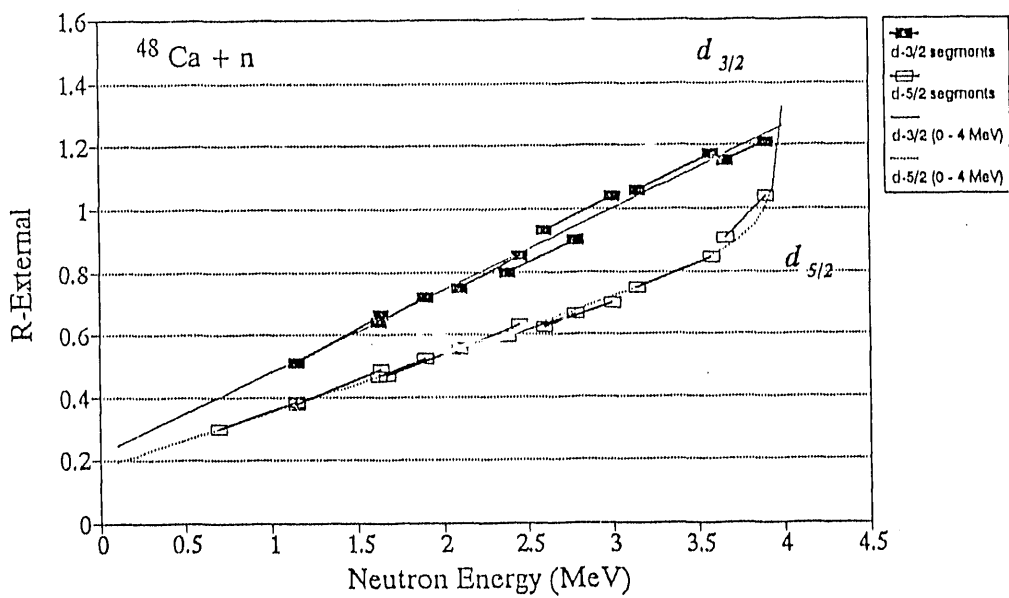


Figure 12

reprint of a book
revised
etc

END

**DATE
FILMED**

416192

I

